2025
12(1), 1185

MATERIALS
NANOSCIENCE

Yttrium incorporation into the tungsten telluride (Y:WTe_2) matrix achieved using three electrode systems

Ernest O. Ojegu[1], Blessing Uyoyou Osolobri[2] Emmanuel Ifeanyichukwu Onyesom[2], Agbakwuru Chijindu Bruno[3], Nawal Alghamdi[5], Imosobomeh L. Ikhioya[5*]

[1]Department of Physics, Delta State University, Abraka. Delta State, Nigeria. [2]Department of Science Laboratory Technology, Delta State Polytechnic, Ogwashi-Uku, Nigeria. [3]Department of Physics/Electronics, Federal Polytechnic, Nekede, Owerri, Imo state. [4]Department of Physics, Faculty of Science, University of Tabuk, Tabuk, 71491, Saudi Arabia. [5]Department of Physics, Federal University Lokoja, Nigeria.

Submitted on: 07-Apr-2025, Accepted and Published on: 14-May-2025

Article

ABSTRACT

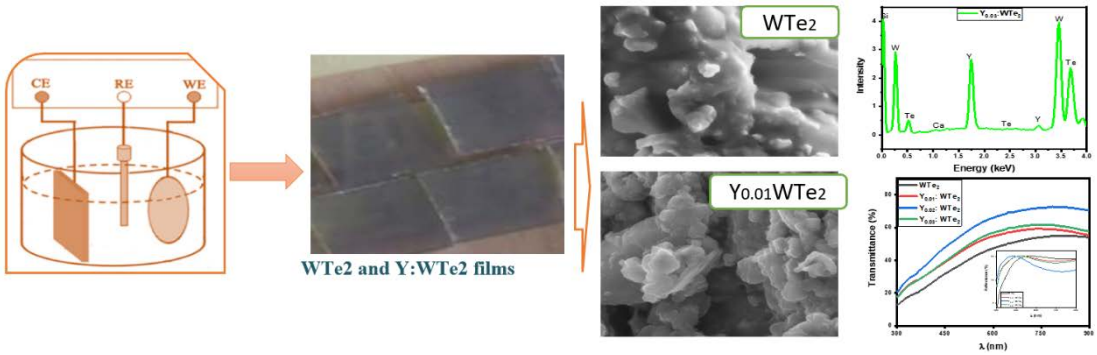

The three-electrode electrochemical deposition technique was used to synthesize Y:WTe2. With a molar concentration of 0.1 mol/g, tellurium dioxide acts as the precursor of zinc tungstate. The molar concentration of the dopant yttrium (III) nitrate hexahydrate ranges from 0.01 to 0.03 mol/g. The XRD patterns of WTe_2 and yttrium-doped tungsten telluride material both display a hexagonal crystal structure. The material exhibited a diffraction peak at (200) with a 2theta angle of 52.034°. At a nanoscale, the material exhibits a specific surface morphology (200 nm scale bar). The typical appearance of materials at this scale is a textured and granular structure on the surfaces. The undoped WTe_2 exhibits well-structured condensed nanoparticles on the FTO glass, along with a clouded white wood precipitate, indicating the formation of tungsten telluride on the FTO substrate. The absorbance of (WTe_2 and various Y-doped compositions) changes with different wavelengths. Stronger light absorption is indicated by higher absorbance, which is correlated with electronic transitions in the material. The energy bandgap of undoped WTe_2 is 1.25 eV, while yttrium-doped WTe_2 shows a range of 1.99 to 1.62 eV bandgap with increasing dopant concentration.

Keywords: tungsten; telluride; bandgap; semimetals; yttrium, three-electrons;

INTRODUCTION

The unique electronic and optical properties of TMDs, or transition metal dichalcogenides, have made them an increasingly intriguing class of 2D materials. Under typical circumstances, TMDs typically have 2H or 1T structures.[1] WTe_2 bulk crystals and powders have a distorted 1T structure (Td) at room temperature, unlike other group VIb TMDs. The lack of atom-by-atom visualization limits our understanding of this distorted 2D layered material system.[2] Tungsten telluride's exceptional structural, electronic, and optical characteristics have positioned it as a highly esteemed transition metal chalcogenide material in recent times. The structure of tungsten telluride comprises a layer of tungsten atoms sandwiched between two layers of tellurium atoms in a distorted 1T crystal structure. The unique structure of Tungsten telluride gives it several fascinating qualities, making it a promising material for various applications in nanostructured materials.[3] The Tungsten telluride lattice exhibits unique electronic phenomena due to strong spin-orbit coupling and broken inversion symmetry, including a non-saturating magnetoresistance effect and the possibility of topological quantum states.[4,5] Various synthesis techniques enable the easy creation of two-dimensional nanostructures, like thin films and nanosheets, due to the layered nature of Tungsten telluride. The enhanced surface-to-volume ratios and quantum confinement effects of these nanostructured forms of Tungsten telluride can result in adjustable electronic, optical, and catalytic properties. Nanostructured Tungsten telluride has been extensively studied for its potential applications in various fields, such as electronics, optoelectronics, energy conversion and storage, and catalysis. Tungsten telluride's high carrier mobility

*Corresponding Author: Dr. I.L. Ikhioya, E-mail: imosobomeh.ikhioya@unn.edu.ng
https://orcid.org/0000-0002-5959-4427

DOI:10.62110/sciencein.mns.2025.v12.1185
URN:NBN:sciencein.mns.2025.v12.1185

https://pubs.thesciencein.org/jmns

and unique magnetoresistance characteristics make it a promising material for next-gen transistors and spintronic devices. High-performance photodetectors and photovoltaic devices have been developed using the strong light-matter interactions and broadband optical absorption of Tungsten telluride nanostructures.[6,7] Tungsten telluride nanostructures have been investigated for their catalytic activity in electrochemical and photochemical reactions, including hydrogen evolution, oxygen reduction, and CO_2 reduction, showcasing their potential in sustainable energy technologies. The research on nanostructured Tungsten telluride is expected to have a growing impact on the development of advanced functional materials and devices, tackling 21st-century technological challenges. The fascinating TMD material's unique properties and versatile applications make it an intriguing subject of study in nanoscience and nanotechnology.[8]

Tungsten telluride, a semi-metal, is famous for its outstanding qualities, such as the highest melting point among elements and impressive mechanical properties at high temperatures. Tungsten's exceptional characteristics make it the top choice for numerous uses, such as light bulb filaments, heating elements, and kinetic energy penetrators.[9] Tungsten's high melting point, low sputtering yield, and resistance to plasma sputtering erosion make it a potential material for plasma-facing components in fusion reactors.[10] However, tungsten has a major drawback in terms of its low ductility at room temperature and high ductile-to-brittle transition temperature.[4,11] The limited ductility of tungsten creates major challenges for its workability and performance in demanding applications. Improving tungsten's mechanical properties could have a significant impact on its production and applications.

John et al[4] present a method to synthesize WTe_2 films in large areas using a synthesis approach. The reaction of pre-deposited W and Te films at 550 °C achieves this. The oxidation of these WTe_2 films in ambient conditions is rapidly self-limiting, as revealed by Sputter X-ray photoelectron spectroscopy. The WTe_2 films comprise micrometer-sized nanobelts that can be isolated and have potential as an alternative to CVT-grown samples. Transmission electron microscopy confirms the low defect densities and high crystallinity of these nanobelts, which also exhibit promising electrical performance. Lee et al [7] conducted experimental and theoretical studies on WTe_2, uncovering a distorted 1T structure and metallic-like transport. The evidence shows that WTe_2 clearly shows metallic behavior. Significant findings have been disclosed about the Raman modes of Td-WTe_2, revealing its susceptibility to oxidation in different environments. These findings suggest that incorporating WTe_2 in electronic devices, particularly field effect transistors, may require reconsideration due to its thermodynamically favored Td form.

Tungsten telluride thin films were synthesized on monocrystal sapphire substrates by Zhang et al[12] using atomic layer deposition and chemical vapor deposition techniques. The films' properties were studied in relation to different tellurization temperatures. At a telluride temperature of 550 °C, the results showed the successful production of tungsten telluride thin films with excellent crystal orientation in (001). The temperature of 570 °C caused tungsten telluride to decompose, leading to the discovery of unsaturated magnetoresistance. In this study, Lu et al. provide atomic resolution images of Td structured WTe_2. The Td structure can be identified in the three main orientations: [100], [010], and [001]. Atomic resolution imaging detects subtle structural distortions that align closely with the optimized structure obtained from ab initio calculations. The calculations revealed that the stabilization of WTe_2 is influenced by both crystal field splitting and charge density wave (CDW) interactions. The CDW interaction prevails, making Td-WTe_2 the most stable structure. The study on WTe2 using atomic resolution STEM and ab initio analysis helped understand the relationship between atomic structure and electronic properties in Td structured TMD materials. WTe_2 nanocrystalline films were made on quartz substrates by Yu et al[13] using magnetron sputtering and chemical vapor deposition methods. Analytical techniques like X-ray Diffraction, Raman spectra, X-ray Photoelectron Spectroscopy, Scanning Electron Microscope, and photoluminescence spectra are used to analyze crystal structure, composition, and morphology. The impact of varying tellurization temperatures and times on WTe_2 thin film properties was studied. At 600 °C for 30 min, they obtained well-crystallized WTe_2 nanocrystalline films. WTe_2 films prepared under this condition exhibited a thermal conductivity of 1.173 $Wm^{-1}K^{-1}$ at 300 K, surpassing that of samples prepared through alternative methods.

The unique electronic, optical, and thermal properties of yttrium-based materials have sparked considerable interest in advanced materials. Doping yttrium-based materials with elements like WTe_2 is a promising approach to boost performance. The addition of yttrium to tungsten telluride (Y:WTe_2) enhances its electrical conductivity, optical bandgap, and structural properties. Electrochemical deposition techniques [14–27] were used to dope yttrium into the tungsten telluride lattice. The addition of yttrium atoms creates defects, vacancies, and alters the structure, affecting the material's properties. The aim of this research is to optimize doping concentration, comprehend property enhancement mechanisms, and explore potential applications of Y:WTe_2 materials in energy storage, catalysis, and optoelectronics. Developing yttrium-doped tungsten telluride materials could open up possibilities for designing innovative functional materials that are more versatile and perform better.

The aim of this study is to present a method for incorporating yttrium into the tungsten telluride matrix (Y:WTe_2) using three electrode systems in electrochemical deposition, specifically for optoelectronic applications. The synthesized material will undergo an analysis of its structural, optical, electrical, and surface morphological properties using different characterization techniques.

Experimental Procedure

2.1. Required Precursors.

The material used to synthesize Y:WTe_2 is zinc tungstate ($ZnWO_4$ 98%), tellurium dioxide (TeO_2 98%), yttrium (III)

nitrate hexahydrate ($Y(NO_3)_3.6H_2O$ 99.8%), hydrochloric acid (HCl), fluorine doped tin oxide (FTO) distilled water. All chemicals were brought from Sigma Aldrich

2.2. Synthesis of Y:WTe_2 material.

The synthesis of Y:WTe_2 involved the utilization of the three-electrode electrochemical deposition technique. The precursor of zinc tungstate ($ZnWO_4$), tellurium dioxide (TeO_2) with a molar concentration of 0.1 mol/g. The dopant yttrium (III) nitrate hexahydrate ($Y(NO_3)_3.6H_2O$) with a molar concentration of 0.01 to 0.03 mol/g. At room temperature, each experiment maintained a steady voltage of 8 V for 60 seconds during the deposition. Controlled parameters were used to test the synthesized undoped and doped WTe_2. In a 50-ml beaker filled with precursors, the deposition process took place with an 8V potential. To establish the electrochemical bath, the dopant molar concentrations needed to be changed from 0.01 to 0.03 mol/g. The bath system was filled with 20 ml of zinc tungstate and tellurium dioxide precursor, along with 10 ml of yttrium (III) nitrate hexahydrate precursor. Heating the resulting samples to 110°C for 60 minutes was done to release the material's tension in Figure 1. Using a Bruker D8-Advance X-ray diffractometer, the structural properties of the films were analyzed. Analysis of the film's surface morphology was performed using MIRA3 TESCAN scanning electron microscopy. Measurements of the wavelength of the optical material from 300 to 900 nm were conducted using the 756S UV-Visible spectrophotometer. The films' additional optical and solid-state properties were determined through optical spectral analysis of the absorbance values.

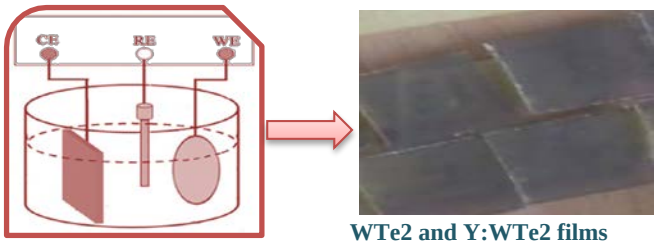

Figure 1: schematic diagram of the three-electrode system of ECD technique.

RESULTS AND DISCUSSIONS

3.1. Structural study of Y:WTe_2 material.

The investigation of the diffraction phase of the material was carried out through a structural study depicted in Figure 2. The XRD patterns of WTe_2 and yttrium-doped tungsten telluride material both display a hexagonal crystal structure. The material exhibited a diffraction peak at (200) with a 2theta angle of 52.034°. The hexagonal phase exhibited well-defined diffraction peaks at specific 2theta angles. The increased surface area, attributed to the material's thickness and higher dopant concentration, may contribute to the greater peaks observed in the spectrum.[1,2,4] Table 1 illustrates the sizes of the material's crystallites. The crystallite size, lattice constants, inter-planar distance, and dislocation densities were determined using Scherrer's equation and are depicted in Table 1. The results were vital for determining the ideal orientation on the (200) plane. Incorporating dopants and the manipulation of crystallite sizes allowed for the compensation of changes in lattice constants and dislocation densities. Changes in lattice sites occur due to a decrease in crystallite size, causing an increase in both 2theta angle and variable lattice constant values. Experimental evidence reveals that the inter-planar spacing differs among various orientation planes. The dopant can occupy the interstitial position due to the distortions caused by its introduction, which alters the lattice structure. The broadening observed at higher 2theta angles can be explained by these aberrations. As the crystallite size increased, the peak broadened at higher 2theta angles. Scherer's mathematical relation and equations (1-3)[28–34] were used to determine the structural properties in Table 1, including the average crystallite size, D, the d-spacing, d, and the lattice constant, a.

$$D = \frac{k\lambda}{\beta\cos\theta} \quad (1)$$

$$d = \frac{\lambda}{2\sin\theta} \quad (2)$$

$$a = d\sqrt{h^2 + k^2 + l^2} \quad (3)$$

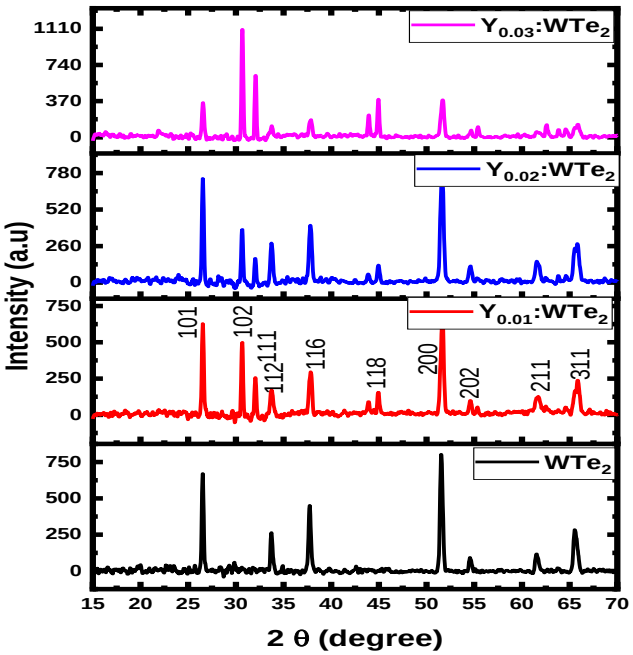

Figure 2: XRD pattern of Y:WTe_2 material.

Table 1: Structural data of Y:WTe_2 material.

Films	2θ (degree)	d (spacing) Å	(Å)	(β)	(hkl)	(D) nm	σ lines/m^2 x 10^{18}
WTe_2	26.211	3.39942	5.8879	25.4105	101	0.0560	9.6898
	30.482	2.93214	5.8642	25.4109	102	0.0565	9.5094
	32.107	2.78736	5.5747	25.4111	111	0.0568	9.4343

	33.302	2.69002	6.0150	25.4112	112	0.0569	9.3768
	37.487	2.39877	5.8757	25.4114	116	0.0576	9.1609
	43.864	2.06370	5.8370	25.4116	118	0.0588	8.7907
	51.237	1.78272	5.0422	25.4117	200	0.0605	8.3061
	54.627	1.67983	5.5713	25.0119	202	0.0614	8.0651
	61.091	1.51667	5.2539	25.0211	211	0.0633	7.5829
	65.186	1.43095	5.3541	25.0212	311	0.0647	7.2571
$Y_{0.01}:WTe_2$	26.519	3.3606	5.8207	25.0105	101	0.0570	9.3753
	30.881	2.8951	5.7903	25.0109	102	0.0575	9.1948
	32.505	2.7541	5.5082	25.0111	111	0.0577	9.1212
	33.701	2.6590	5.9458	25.0112	112	0.0579	9.0649
	37.882	2.3746	5.8167	25.0114	116	0.0586	8.8539
	44.862	2.0200	5.7136	25.0116	118	0.0600	8.4559
	52.034	1.7572	5.7136	25.0117	200	0.0600	8.4559
	54.824	1.6742	5.8282	25.0119	202	0.0617	7.9928
	61.799	1.5009	5.7998	25.0211	211	0.0624	7.8050
	65.983	1.4155	5.6161	25.0212	311	0.0646	7.2924
$Y_{0.02}:WTe_2$	26.519	3.3606	5.8207	25.2105	101	0.0565	9.5259
	30.881	2.8951	5.7903	25.2109	102	0.0571	9.3424
	32.505	2.7541	5.5082	25.2111	111	0.0573	9.2677
	33.701	2.6590	5.9458	25.2112	112	0.0575	9.2104
	37.882	2.3746	5.8167	25.2114	116	0.0581	8.9961
	44.862	2.0200	5.7136	25.2116	118	0.0595	8.5916
	52.034	1.7572	5.7136	25.2117	200	0.0595	8.5917
	54.824	1.6742	5.8282	25.2119	202	0.0612	8.1211
	61.799	1.5009	5.7998	25.2211	211	0.0619	7.9303
	65.983	1.4155	5.6161	25.2212	311	0.0641	7.4095
$Y_{0.03}:WTe_2$	26.519	3.3606	5.8207	25.6105	101	0.0556	9.8306
	30.881	2.8951	5.7903	25.6109	102	0.0562	9.6412
	32.505	2.7541	5.5082	25.6111	111	0.0564	9.5641
	33.701	2.6590	5.9458	25.6112	112	0.0566	9.5050
	37.882	2.3746	5.8167	25.6114	116	0.0572	9.2838
	44.862	2.0200	5.7136	25.6116	118	0.0586	8.8664
	52.034	1.7572	5.7136	25.6117	200	0.0586	8.8665
	54.824	1.6742	5.8282	25.6119	202	0.0602	8.3809
	61.799	1.5009	5.7998	25.6211	211	0.0610	8.1839
	65.983	1.4155	5.6161	25.6212	311	0.0631	7.6464

3.2. Surface morphological study of Y:WTe_2 material.

Figure 3 shows the surface image of the tungsten telluride and yttrium doped tungsten telluride. At a nanoscale, the material exhibits a specific surface morphology (200 nm scale bar). The typical appearance of materials at this scale is a textured and granular structure on the surfaces. The undoped WTe_2 exhibits well-structured condensed nanoparticles on the FTO glass, along with a clouded white wood precipitate, indicating the formation of tungsten telluride on the FTO substrate. The addition of the yttrium to the tungsten telluride matrix altered the synthesized material's lattice parameters and energy bandgap. Increasing the doping concentration leads to an increase in the grain size of the material, demonstrating that incorporating yttrium into the tungsten telluride matrix improves the analysis of its surface morphology. This is evident in the structural analysis of the

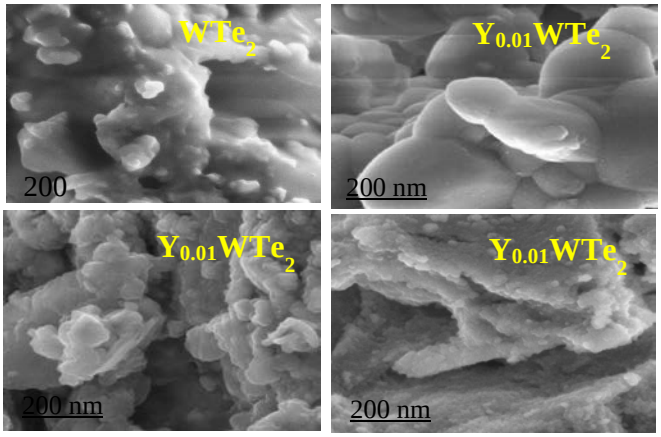

Figure 3: surface micrograph of Y:WTe_2 material.

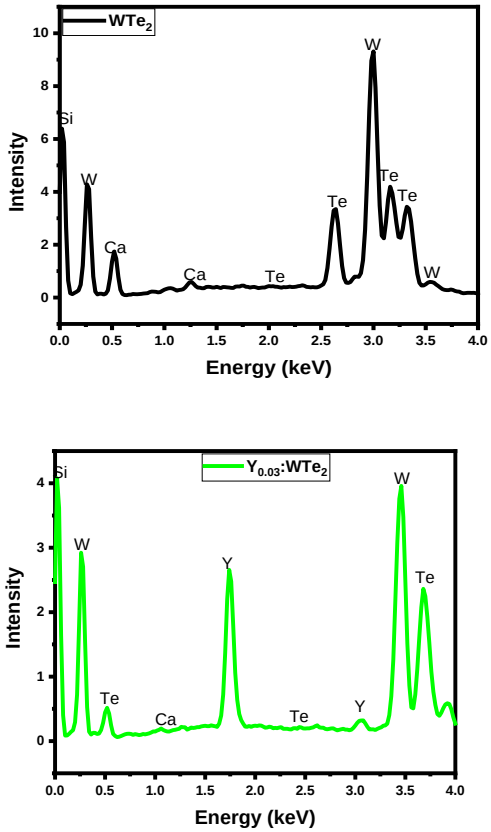

Figure 4: EDX spectrum of Y:WTe2 material.

material. The addition of yttrium resulted in alterations in grain size. Increased levels of yttrium lead to smaller grains as the nucleation and growth processes change during material synthesis. By introducing yttrium, the surface roughness was decreased, leading to enhanced material surface micrograph. Yttrium plays a role in stabilizing particular phases of WTe_2, which alters its overall morphology. This stabilization caused structures to become more homogeneous. Yttrium has influenced the material's electronic properties, potentially causing defects or vacancies. Yttrium doping modifies the chemical composition locally, resulting in changes to electronic structure and surface

properties. The performance of WTe_2 in applications such as thermoelectric devices is affected by these morphological changes, which are crucial for efficiency due to the role of surface characteristics. Yttrium doping alters the surface morphology of WTe_2, impacting its physical properties and potential applications. The elemental analysis of tungsten telluride and yttrium doped tungsten telluride is shown in Figure 4. All the elements we anticipated were detected in the EDX spectrum. The FTO substrate used for synthesis is responsible for the other element in the spectrum. Table 2 provides the atomic weight percentage of the material.

Table 2: EDX analysis atomic weight percentages of Y:WTe_2 material.

WTe_2		**$Y_{0.03}$:WTe_2**	
Component	Atomic Weight (%)	Component	Atomic Weight (%)
W	58.3	W	52.1
Te	29.0	Te	26.2
Ca	3.1	Ca	3.1
Si	9.6	Si	9.6
-		Y	9

3.3. Absorption study of tungsten telluride and yttrium doped tungsten telluride.

The absorbance of tungsten telluride and yttrium doped tungsten telluride is shown in Figure 5a. The absorption of tungsten telluride and yttrium-doped tungsten telluride decreases as visible light increases, indicating photon absorption by the material. When compared to yttrium doping, the WTe_2 material exhibits higher absorbance on the plot. Lowering the dopant content affects the material's matrix, indicating the critical role of the dopant. The absorbance of (WTe_2 and various Y-doped compositions) changes with different wavelengths. Stronger light absorption is indicated by higher absorbance, which is correlated with electronic transitions in the material. Y-doped WTe_2 material exhibits noticeable variations in absorbance compared to undoped WTe_2, indicating that yttrium doping modifies the electronic structure [1,5,13]. Y-doped materials show increased absorbance in specific regions, suggesting improved electronic states or reduced bandgap. Shifting absorbance peaks (either shorter or longer wavelengths) in Y-doped material compared to undoped WTe_2 suggest alterations in bandgap energy, influencing optical properties. The optical properties obtained from this graph are essential for photonics and optoelectronics applications. The potential applications of yttrium dopant absorbance include devices such as sensors, solar cells, or other optoelectronic applications. Figure 5b shows the transmittance of tungsten telluride and yttrium doped tungsten telluride. Tungsten telluride and yttrium-doped tungsten telluride show higher transmittance with increasing visible light, suggesting material's photon absorption. The transmittance of the WTe_2 material is lowest when compared to yttrium doping. The dopant plays a critical role in the material's matrix, as shown by the impact of

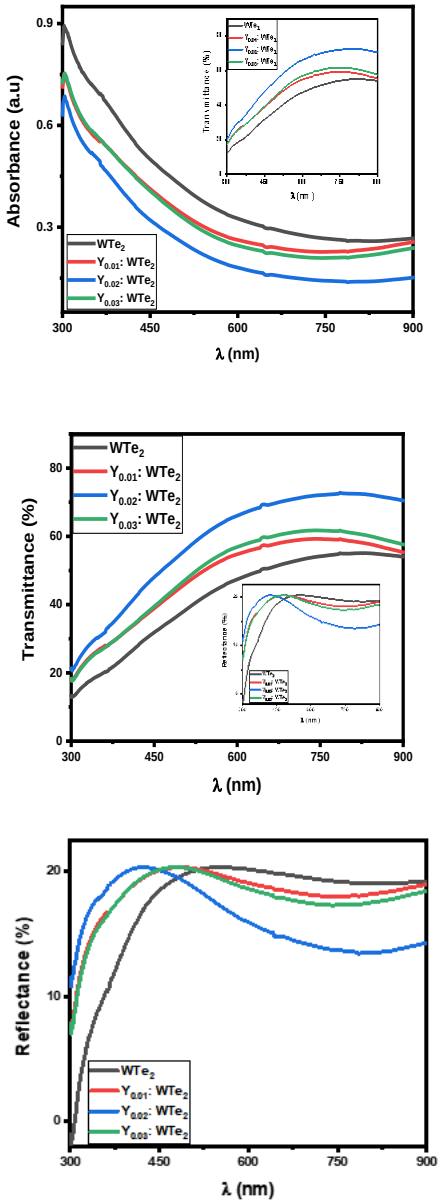

Figure 5: absorption (a), transmittance (b), and reflectivity (c).

lowering its content. The transmittance of (WTe_2 and different Y-doped compositions) varies with different wavelengths. Among the transmittance values in the plot, the yttrium dopant had the highest recorded transmittance. The transmittance is enhanced by yttrium doping in the visible range. In the infrared and ultraviolet ranges, the impact is greater as transmittance is significantly altered by modified absorption edges. The optical properties undergo subtle changes with introducing yttrium at lower dopant levels. The effects become more noticeable at higher levels, potentially causing a significant decrease in transmittance from increased absorption. The addition of yttrium to WTe_2 results in intricate variations in transmittance, influenced by the concentration of doping, wavelength, and resulting modifications in the electronic structure. Tailoring the material's properties is crucial for specific optoelectronic applications. The reflectance of tungsten telluride and yttrium doped tungsten telluride is

shown in Figure 5c. Increasing visible light leads to higher reflectance in tungsten telluride and yttrium-doped tungsten telluride, indicating photon absorption in the material [1,5,13]. The WTe_2 material exhibits a higher reflectance compared to yttrium doping. The presence of yttrium doping result in an increase or decrease in reflectance as wavelength increases in the visible region of the spectral. Higher levels of yttrium lead to more significant alterations in reflectance, which result in increased scattering and absorption, ultimately reducing overall reflectance. Enhanced reflectance properties increase optical sensor sensitivity. Yttrium doping in WTe_2 causes notable variations in reflectance, influenced by the concentration of doping, wavelength, and modifications to the material's optical properties.

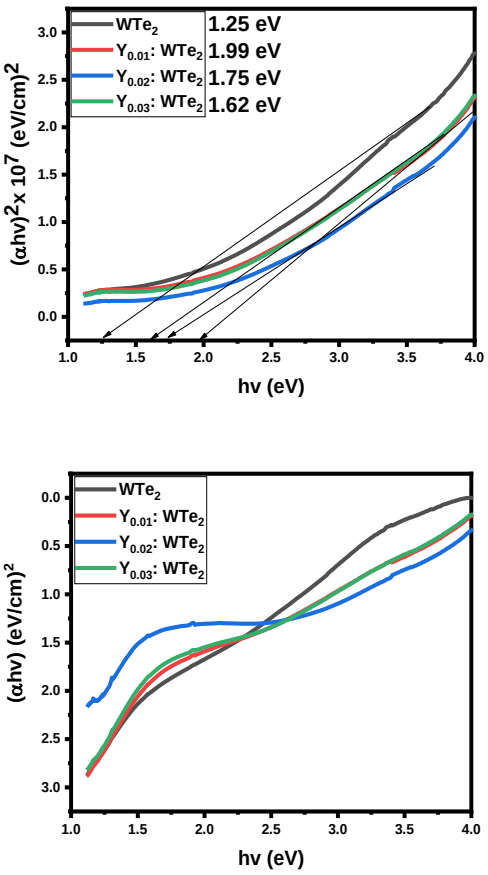

Figure 6: bandgap (a) and absorption coefficient (b).

The plot of absorption coefficient square as a function of photon energy was used to determine the energy bandgap of tungsten telluride and yttrium-doped tungsten telluride in Figure 6 (a). The energy bandgap of undoped WTe_2 is 1.25 eV, while yttrium-doped WTe_2 shows a range of 1.99 to 1.62 eV bandgap with increasing dopant concentration. Figure 6 (b) shown that as the photon energy increases, the absorption coefficient of the material increases across the board. Yttrium doping alters the bandgap and, impacts the optical properties of WTe_2. The wavelengths of absorbed light are affected by the shift in energy

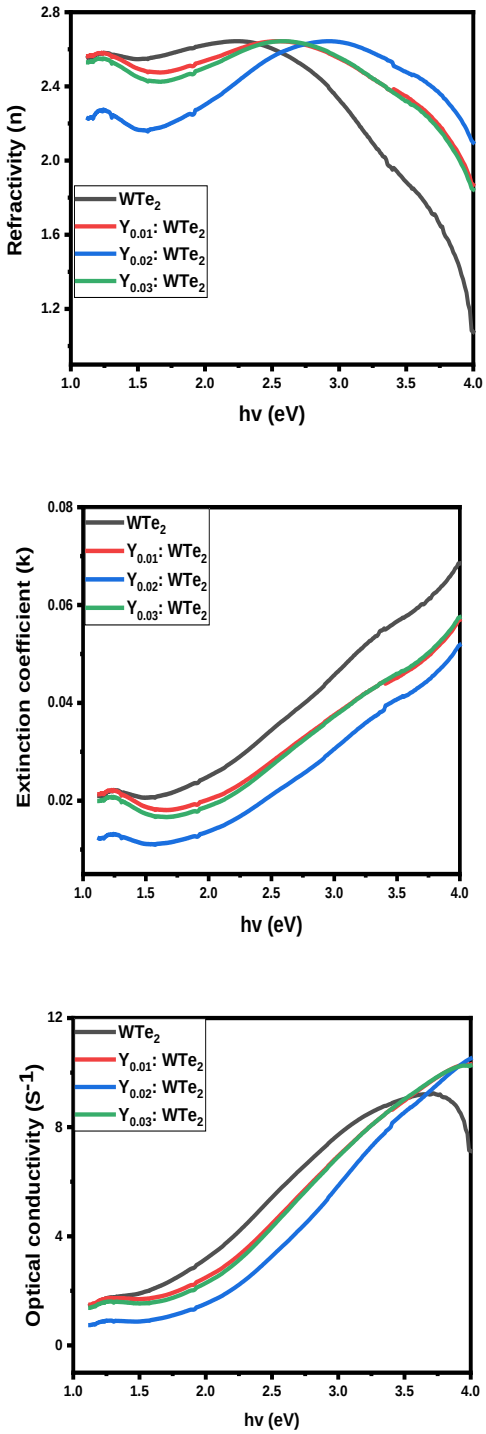

Figure 7: refractivity (a), extinction coefficient (b), and optical conductivity (c)

bandgap towards the absorption edge. Photoconductivity and other optoelectronic properties are influenced by the material's response to light, which is determined by the bandgap [32,35].The bandgap of WTe_2 can be modified for optoelectronic applications by incorporating the yttrium. By adjusting the bandgap, it becomes possible to create devices such as photodetectors, solar

cells, and LEDs. The performance of thermoelectric materials is improved by optimizing the Seebeck coefficient and electrical conductivity through a modified bandgap. The energy bandgap of WTe_2 is significantly affected by yttrium doping, influenced by the concentration and specific electronic interactions. By making this modification, it becomes possible to tailor the material's properties for different optoelectronic and semiconductor uses.

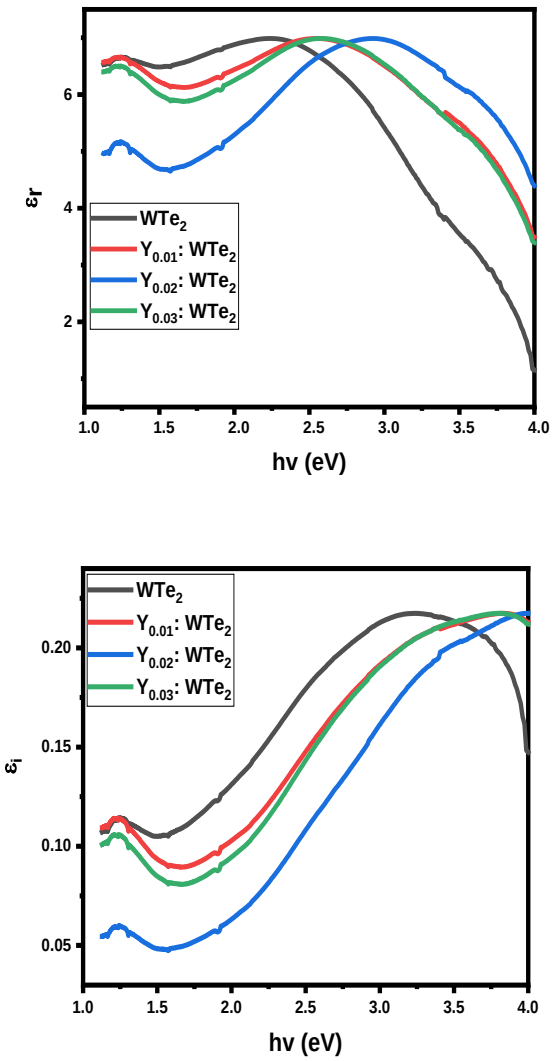

Figure 8: real (a) and imaginary (b) dielectric constant.

Figure 7 (a) displays the refractivity of the tungsten telluride and yttrium doped tungsten telluride. The refractivity of tungsten telluride and yttrium-doped tungsten telluride increases with higher visible light, suggesting photon absorption in the material. Yttrium doping yields a lower refractivity than the WTe_2 material. The addition of yttrium doping can cause refractivity to either increase or decrease with increasing wavelength in the visible spectral region. Increased levels of yttrium cause more notable changes in refractivity, leading to higher scattering and absorption and ultimately decreasing overall refractivity. Increasing refractivity enhances sensitivity of optical sensors. Doping WTe_2 with yttrium leads to significant changes in refractivity, which depend on doping concentration, wavelength, and alterations to optical properties. The extinction coefficient and optical conductivity increase with increasing photon energy in Figure 7 (b & c). Yttrium dopant concentration is responsible for the observed decreases in the material. Figure 8 (a & b) depicts the real and imaginary dielectric constant of the material.

Conclusions

Using the three-electron system of ECD technique, we have successfully synthesized yttrium-doped WTe_2. The XRD patterns of WTe_2 and yttrium-doped tungsten telluride material both display a hexagonal crystal structure. The material exhibited a diffraction peak at (200) with a 2theta angle of 52.034°. At a nanoscale, the material exhibits a specific surface morphology (200 nm scale bar). The typical appearance of materials at this scale is a textured and granular structure on the surfaces. The undoped WTe_2 exhibits well-structured condensed nanoparticles on the FTO glass, along with a clouded white wood precipitate, indicating the formation of tungsten telluride on the FTO substrate. The absorbance of (WTe_2 and various Y-doped compositions) changes with different wavelengths. Stronger light absorption is indicated by higher absorbance, which is correlated with electronic transitions in the material. The energy bandgap of undoped WTe_2 is 1.25 eV, while yttrium-doped WTe_2 shows a range of 1.99 to 1.62 eV bandgap with increasing dopant concentration.

Acknowledgment

Our gratitude goes out to the authors for their important financial backing that greatly contributed to the success of the research.

Author contribution statement

Ernest O. Ojegu, Blessing Uyoyou Osolobri Emmanuel Ifeanyichukwu Onyesom, Agbakwuru Chijindu Bruno : methodology, conceptualization, data curation, data collection, Nawal Alghamdi, Imosobomeh L. Ikhioya: first-draft writing, software, reviewing, and editing. Imosobomeh L. Ikhioya, Nawal Alghamdi: supervisor, investigation and visualization. All authors approved the submission of the manuscript.

Disclosing conflicting interests.

The authors of this paper assert that there were no personal or financial conflicts that could have influenced the study.

References and notes

1. A. Giri, H. Yang, W. Jang, et al. Synthesis of Atomically Thin Transition Metal Ditelluride Films by Rapid Chemical Transformation in Solution Phase. *Chemistry of Materials* **2018**, 30 (7), 2463–2473.
2. N. Lu, C. Zhang, C.H. Lee, et al. Atomic and Electronic Structures of WTe2 Probed by High Resolution Electron Microscopy and ab Initio Calculations. *Journal of Physical Chemistry C* **2016**, 120 (15), 8364–8369.
3. G. Sanyal, A. Vaidyanathan, C.S. Rout, B. Chakraborty. Recent developments in two-dimensional layered tungsten dichalcogenides

based materials for gas sensing applications. *Materials Today Communications* **2021**, 28.
4. J.B. Mc Manus, C. Ilhan, B. Balsamo, et al. Synthesis of tungsten ditelluride thin films and highly crystalline nanobelts from pre-deposited reactants. *Tungsten* **2020**, 2 (3), 321–334.
5. C. Ren, Z.Z. Fang, M. Koopman, et al. Methods for improving ductility of tungsten - A review. *International Journal of Refractory Metals and Hard Materials* **2018**, 75, 170–183.
6. M. Fang, X. Liu, J. Liu, et al. Improved Thermal Anisotropy of Multi-Layer Tungsten Telluride on Silicon Substrate. *Nanomaterials* **2023**, 13 (12).
7. C.H. Lee, E.C. Silva, L. Calderin, et al. Tungsten Ditelluride: A layered semimetal. *Scientific Reports* **2015**, 5, 1–8.
8. Y. Zhang, Z. Wang, J. Feng, et al. Synthesis and electromagnetic transport of large-area 2D WTe2 thin film. *Journal of Semiconductors* **2022**, 43 (10).
9. I. Chauhan, M. Kaur, K. Singh, et al. Temperature-dependent photoconductivity studies of WTe2/MoS2 nanocomposite thin film. *Surfaces and Interfaces* **2022**, 29.
10. T. V. Mc Knight, T.H. Choudhury, K. Wang, A. Bansal, J.M. Redwing. MOCVD Growth of Tungsten Ditelluride Thin Films. *Journal of Crystal Growth* **2024**, 625.
11. S. Surnev, F.P. Netzer. Tungsten and molybdenum oxide nanostructures: Two-dimensional layers and nanoclusters. *Journal of Physics Condensed Matter* **2022**, 34 (23).
12. Y. Zhang, Z. Wang, J. Feng, et al. Synthesis and electromagnetic transport of large-area 2D WTe2 thin film. *Journal of Semiconductors* **2022**, 43 (10).
13. Z. Yu, R. Tao, J. Guo, S. Feng, Y. Wang. Direct Growth of Low Thermal Conductivity WTe2 Nanocrystalline Films on W Films. *Nanomaterials* **2024**, 14 (5).
14. I.L. Ikhioya, A.C. Nkele. Properties of electrochemically deposited NiTe films prepared at varying dopant concentrations of molybdenum. *Journal of Materials Science: Materials in Electronics* **2023**, 34 (21).
15. I.L. Ikhioya, A.C. Nkele. A Novel Synthesis of Hydrothermally Prepared Europium Sulfide and Cerium Sulfide Nanomaterials Doped with Yttrium. *Arabian Journal for Science and Engineering* **2023**.
16. I.L. Ikhioya, I. Rufus, N.I. Akpu. Influence of temperature on energy band gap and other properties of undoped and cadmium doped manganese sulphide (MnS:Cd) synthesized for photovoltaic and optoelectronic application. *Asian Journal of Nanoscience and Materials* **2022**, 5 (2), 88–97.
17. I.L. Ikhioya, E.U. Onoh, D.N. Okoli, A.J. Ekpunobi. Impact of bismuth as dopant on ZnSe material syntheses for photovoltaic application. *Materials Research Innovations* **2023**, 00 (00), 1–9.
18. I.L. Ikhioya, C.O. Ugwuoke, D.N. Okoli, et al. Effect of cobalt on the photovoltaic properties of zinc selenide thin film deposited on fluorine-doped tin oxide (FTO) via electrochemical deposition technique. *Current Research in Green and Sustainable Chemistry* **2022**, 5 (May), 100328.
19. I.L. Ikhioya, G.M. Whyte, A.C. Nkele. Temperature-modulated nanostructures of ytterbium-doped Cobalt Selenide (Yb-CoSe) for photovoltaic applications. *Journal of the Indian Chemical Society* **2023**, 100 (1), 100848.
20. I.L. Ikhioya, C.O. Ugwuoke, F.U. Ochai-ejeh, et al. Optimisation of temperature regulator on spray pyrolysis cobalt selenide doped erbium (CoSe : Er) semiconductor material for photovoltaic application. *Materials Research Innovations* **2023**, 00 (00), 1–8.
21. B.C.N. Obitte, I.L. Ikhioya, G.M. Whyte, et al. The effects of doping and temperature on properties of electrochemically deposited Er3+ doped ZnSe thin films. *Optical Materials* **2022**, 124 (December 2021), 111979.
22. S.O. Samuel, M.L.E. Frank, E.P. Ogherohwo, et al. Influence of Deposition Voltage on Strontium Sulphide Doped Silver for Optoelectronic Application. *East European Journal of Physics* **2023**, 2023 (1), 189–196.
23. S.O. Samuel, M.F. Lagbegha-ebi, E.P. Ogherohwo, I.L. Ikhioya. Improve physical properties of zirconium doped strontium sulphide for optoelectronic purpose. *Results in Optics* **2023**, 13 (June), 100518.
24. I. Rufus, A. Peter, S.O. Aisida, I.L. Ikhioya. Results in Optics Influence of manganese molarity incorporation on manganese silver sulphide semiconductor material for photovoltaic applications. *Results in Optics* **2023**, 12 (February), 100464.
25. K.I. Udofia, I.L. Ikhioya, A.U. Agobi, D.N. Okoli, A.J. Ekpunobi. Effects of zirconium on electrochemically synthesized tin selenide materials on fluorine doped tin oxide substrate for photovoltaic application. *Journal of the Indian Chemical Society* **2022**, 99 (10), 100737.
26. K.I. Udofia, I.L. Ikhioya, D.N. Okoli, A.J. Ekpunobi. Impact of doping on the physical properties of PbSe chalcogenide material for photovoltaic application. *Asian Journal of Nanoscience and Materials* **2023**, 6 (2), 135–147.
27. E.O. Ojegu, S.O. Samuel, M.O. Osiele, G.E. Akpojotor, I.L. Ikhioya. Optimisation of deposition voltage of zirconium-doped chromium telluride via typical three-electrode cell electrochemical deposition technique. *Materials Research Innovations* **2023**, 00 (00), 1–9.
28. A.I. Agbrara, E.O. Ojegu, M.O. Osiele, I.L. Ikhioya. Electrochemically Synthesize SrSe/ZrSe Heterostructure Material for Photovoltaic Application. *Advanced Journal of Chemistry, Section A* **2023**, 6 (4), 401–411.
29. A.U. Agobi, A.I. Ikeuba, A.J. Ekpunobi, et al. Optical and structural properties of graphene oxide-incorporated polyvinylpyrrolidone/copper ternary nanocomposites (PVP/Cu/GO) films. *Revista Mexicana de Fisica* **2023**, 69 (3), 1–9.
30. N.I. Akpu, C.A. Sylvanus, E.C. Nwaokorongwu. Modulation of the physical properties of spray-deposited cobalt selenide nanofilm via yttrium doping for photovoltaic purposes . **2023**, 14 (11), 1230–1244.
31. N. Akpu, U. Okpechi, N. Elizabeth, et al. Impact of temperature difference on the features of spray deposited yttrium doped cobalt selenide (YCoSe) thin films for photovoltaic application. *African Scientific Reports* **2023**, 2, 143.
32. I.L. Ikhioya, A.C. Nkele. Green synthesis and characterization of aluminum oxide nanoparticle using neem leaf extract (Azadirachta Indica). *Hybrid Advances* **2024**, 5 (November 2023), 100141.
33. I.L. Ikhioya, C.O. Ugwuoke, R.M. Obodo, et al. Influence of precursor pH on Bi doped ZnSe material via electrochemical deposition technique. *Applied Surface Science Advances* **2022**, 9 (November 2021), 100232.
34. C. Uchechukwu, A. Osita, J. Chukwuemeka, I. Lucky, O. Odira. Investigating the influence of natural dye extracts from Ocimum gratissimum , Solanum melongena , Piper guineese , and their blend in the fabrication of perovskite solar cells. *Hybrid Advances* **2024**, 6 (April), 100198.
35. I.L. Ikhioya, N.Z. Ali, S. Tahir, et al. Electrochemical engineering of ZIF-7 electrode using ion beam technology for better supercapacitor performance. *Journal of Energy Storage* **2024**, 90 (PA), 111833.